AN EXPERIMENTAL DETERMINATION AND NUMERICAL ANALYSIS OF A LOITER MUNITION UNMANNED AERIAL VEHICLE SYSTEM

Yazarlar (Authors): Tamer Saraçyakupoğlu [iD]*, Heyzem Doğukan Delibaş [iD], Ahmet Devlet Özçelik [iD]

Araştırma Makale/ Research Article

AN EXPERIMENTAL DETERMINATION AND NUMERICAL ANALYSIS OF A LOITER MUNITION UNMANNED AERIAL VEHICLE SYSTEM

Tamer Saraçyakupoğlu[a] *, Heyzem Doğukan Delibaş[b] , Ahmet Devlet Özçelik[b]

[a]* Turkish Aerospace Industries, Turkey
[b]Istanbul Gelisim University, Department of Aircraft Maintenance and Repair, Turkey

*Correspondent Author: dr.tamer@tamersaracyakupoglu.com.tr

ABSTRACT

This paper experimentally determinates the calculation of an Unmanned Aerial Vehicle (UAV) and analyzes the design criteria within four different scenarios. The UAV to be designed is a loiter munition UAV system. A mobile or equipment such as a parachute and/or airbag. The UAV may be operable day and night conditions, capable of 2-3 hours of flight hours, and will be launched from a catapult. The UAV navigation system is compact and easily controlled by a personal Global Positioning System (GPS). The mentioned UAV will have a vast operational capability, especially for defense and border security activities since it is equipped with advanced avionics and a small physical footprint for covert operations. As a consequence of this research, it can be claimed that the UAV's mid-wing, twin-tail, and relatively light body will have three axis stability and offer numerous benefits, particularly in terms of operational cost.

Keywords: Mission Profile, Speed Condition, Weight Calculation, Unmanned Aerial Vehicle (UAV), Wing Design, Tail Design

1. INTRODUCTION

A detailed literature research has been executed for analyzing the manufacturing methodology of a UAV in terms of parametric determination. In a similar segment to the subject of this paper, the six competitor UAVs have been investigated.

1.1. Types of Loiter Munition UAV Systems

A list of the characteristic of the requirements of six competitor UAVs was obtained, compared, and therefore provided. The geometric characteristics of the competitor UAVs are listed and shown in tables. Tables are used for comparing the features. Average values of the specifications and given required parameters are compared. The selected UAVs are; STM Alpagu, XQ-06 Fi, Kalashnikov's Kub, Orbiter 1K, IAI Green Dragon, and Raytheon Coyote. The requirements for the selected competitor UAVs are; Range (Km), Task Time (min), Maximum Altitude (feet), Maximum Speed (Km/h), Stall Speed (Km/h), Weight (Kg), Payload (Kg), Wingspan (m), and Length (m). The comparison assumpted requirements and threshold values are provided in Table 1.

Table 1. The comparison requirements and threshold values [1-7].

Requirement	Threshold Value
Task Time (Min)	60 min
Range (Km)	50 km
Maximum Altitude (Feet)	914.4 m (3000 feet)
Maximum Speed (Km/h)	120 km/h (33.3 m/s)
Cruise Speed (Km/h)	80 km/h
Stall Speed (Km/h)	70 km/h (19.4 m/s)
Weight (Kg)	12 kg
Payload (Kg)	2 kg
Wingspan (m)	3 m

The mainframe of this study is to calculate the mission profile parameters while comparing the UAVs that operate in similar conditions. The below-given UAVs are selected in terms of comparison.

1.1.1. Alpagu

Alpagu, a Portable Fixed Wing Intelligent Ammunition System (PFWIS) is a fixed-wing portable smart ammunition system that can be carried by a single soldier, can operate autonomously or remotely, designed for both reconnaissance and surveillance at a tactical level and to hit targets outside the line of sight with high accuracy. It can be used effectively day and night against fixed or moving targets with the help of embedded and real-time image processing and deep learning algorithms. The operative system consists of "Fixed Wing Intelligent Ammunition System", "Launch Launcher" and "Ground Control Station" components [1].

1.1.2. XQ-06 Fi

Developed by Kartal Defense Technologies company with Hacettepe University, the XO-06 "Fi" Entangled Ammunition "mini unmanned aerial vehicle carries 500 grams of plastic explosives. The mini unmanned aerial vehicle launched from a tube destroys itself and the target by diving kamikaze to the desired area with the camera system on it via ground control devices. It is a mini unmanned aerial vehicle carried on the back, controlled by only one personnel, starting its flight with the help of a mortar-like launcher, wirelessly transmitting what it sees on its camera to the ground control station, and containing plastic explosives in its body [2].

1.1.3. Kalashnikov's Kub

Kub is manufactured by the famous Russian defense contractor Kalashnikov Concern whose name is mainly known the for procurement of infantry weapons for Russian Ground Forces. The aforementioned security has generated a drone capable of holding a small explosive device and diving into its target in order to blow itself and the target into small bits. The Kub which is manufactured by Kalashnikov is in kamikaze status meant to fly under the radar of conventional air-defense systems [3].

1.1.4. Orbiter 1K

The Orbiter Mini UAV named Orbiter 1K is a unique, lightweight and well-equipped UAV designed and produced by the Aeronautics Company (Israeli company Aeronautics Defense Systems) for both security and military operations. It was first developed in 2015 and since then, it has been used in the Middle East. It is in the UAV market especially for Non-Line of Sight (NLOS) operations called "Over The Hill" reconnaissance missions. The Orbiter 1K is also used for, Intelligence, Surveillance, Target Acquisition, and Reconnaissance (ISTAR) missions, urban warfare activities, low-intensity conflicts, and as well as any close-range missions [4, 5].

1.1.5. IAI Green Dragon

The Green Dragon is a tactical, low-cost loitering munition that was manufactured for providing small the significant situational awareness and firepower to ground units and special operations forces within a compact envelope. With its unique storage, transportation, and launching mechanism that is customized for launching from a sealed canister. Besides, it was designed for being carried on a small vehicle up to 12-16 Green Dragon units upon request. IAI Green Dragon's propelling system is a pusher configuration and it can be easily controlled and operated by a tablet-sized electronic device that is equipped with a low-power data link [6].

1.1.6. Raytheon Coyote

The Raytheon Coyote was manufactured by the Raytheon Company with its significant capability of autonomous swarms. It is relatively small and has to expand the fuselage feature. After launching from a sonobuoy canister, it flies with the deploying wings during the early flight phase. The interchangeability of payload is its unique feature. The Raytheon Coyote can operate for up to one hour. So far, it has been used by the National Oceanographic and Atmospheric Administration (NOAA) for hurricane tracking in the civilian field. On the military side, it has been operated by the United States Air Force and Army as an intelligence, surveillance, and reconnaissance asset, and for kinetic payloads delivery [7]. Performance requirements of the aforementioned UAVs are presented in Table 2.

Table 2. Performance Requirements.

| Requirements | The UAV Model | | | | | | |
	Alpagu	XQ-06 Fi	Kalashnikov's Kub	Orbiter 1K	IAI Green Dragon	Raytheon Coyote	Average
Task Time (min)	10	15	30	150	90	120	69.17
Range (km)	5	12	64	100	300	130	101.83
Maximum Altitude (feet)	400	15092		8000	5000	30000	11698.4
Cruise Speed (km/h)	80	75	80	55		102	78.4
Maksimum peed (km/h)	120	125	130	130	203.72	130	139.79
Weight (kg)	1.9	3,5		13	15	5.9	7.86
Payload (kg)	0.15	0,75	3	2	2,5	0.9	1.55
Wingspan (m)	0.65	1,5	1.19	2.90		1.5	1.55
Length (m)	0.125		0.94			0.91	0.66

In a conclusion, some information concerning each UAV is found regarding the properties given to us. Besides, tables are generated for all of the properties, and the average values of these properties too are obtained and are also shown. Tables make easy the way of comparing each UAV's properties to the other. This study gives information and specifications for the chosen UAVs. Finally, by comparing each UAV, we get more knowledge about all six UAVs and know better about their properties and specifications and we are now able to discuss and talk about all six UAVs mentioned above.

2. MATERIAL AND METHOD
In this study, according to the given mission, the mission profile of the A/C which is asked to design is sketched. The initial estimation of the design Take-Off Gross Weight (TOGW) based on the mission profile is performed by taking the average values of the 6 aircraft found. Payload trade and range trade for the mission profile cruise mission is calculated and the results are plotted.

During the design phase the following preliminary design evaluation items are essential to be considered as main requirements [8]

- Development of detailed aerodynamic shape
- Weight and balance Layout of major load paths
- Flight stability
- Evaluation of unique aerodynamic specifications
- Platform overall flight performance
- Mission characteristic
- Certification and validation issues
- Achieving ability of mission envelope
- Easy manufacturability specifications
- Easy maintainability specifications
- Production and operational cost estimation

In general, the followings are relevant to the provided above calculation items.

2.1. Mission Profile
The simple cruise mission profile figure is obtained for the given mission profile for the parameters given as follows and in Figure 1 by Raymer et al [9].
- Take off at mean sea level (MSL)
- Climb to 3000 feet.
- Perform 100 km of flight at 3000 feet.
- Descent to MSL
- Landing and stop
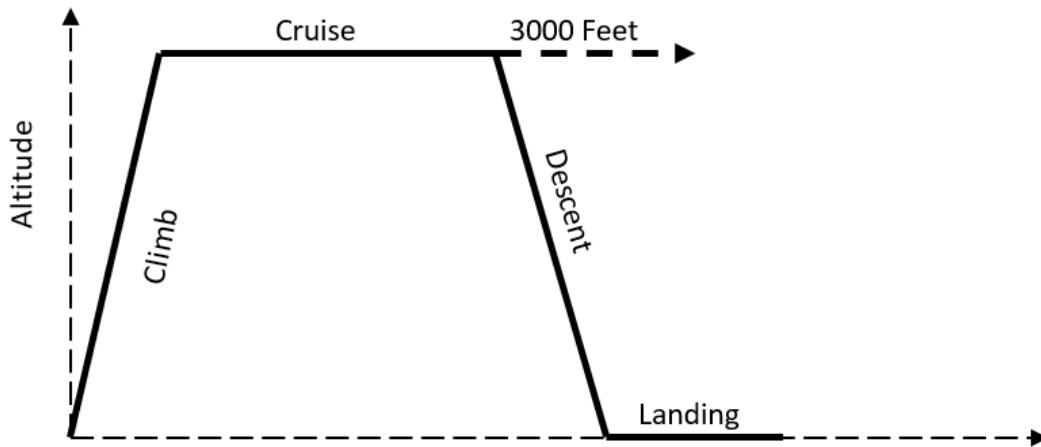
Figure 1. Mission Profile.

2.2. Gross Weight Calculation

One of the most important descriptions is gross weight which the pilot is allowed to attempt to take off, due to structural or other limits.
The general formula for W_0 is known as;

$$W_0 = \frac{W_{Payload}}{(1-\frac{W_f}{W_0}-\frac{W_e}{W_0})} \qquad (1)$$

Where the overall weight is W_0, W_f is the weight of the fuel and the empty weight is We. Also, the Fuel Fraction Weight Ratio is W_f/W_0. In this way, as given in Table 3, the gross weight was determined iteratively.

Table 3. Gross Weight Calculating Iteration.

W_0 (lbs)	W_{crew} (lbs)	$W_{payload}$ (lbs)	W_f (lbs)	W_f/W_0	W_e/W_0	W_0	Difference	W_0 (kg)
16.5	0	4.41	0	0	0.781	20.182	3.682	7.4745
18	0	4.41	0	0	0.778	19.874	1.874	8.154
19.5	0	4.41	0	0	0.775	19.599	0.099	8.8335
21	0	4.41	0	0	0.772	19.353	-1.647	9.513
22.5	0	4.41	0	0	0.769	19.129	-3.371	10.1925

Firstly, W_0 estimated value is given as 40 lbs which is the average of the chosen 6 UAVs. Results of W_0 are found by using computer-based calculations code. It is noteworthy that a W_0 estimated value is needed to calculate for real W_0. However, no matter what the chosen W_0 estimated value is, the W_0 calculated value will always be the same. Each time a W_0 calculated value is iterated, the code sums W_0 guess and W_0 calculated and divides them by 2 to find the new W_0 estimated value. By using this method, with each step the code gets closer to the real W_0 value. Eventually, after 5 iterations, W_0 calculated is found to be 47 lbs which is very close to the W_0 estimated value of 46.6 lbs. It

could be used for the first W_0 estimated value and will be found the same result, however probably with a different number of iterations.

2.3. Payload Trade

Payload trade can be evaluated to determine the increase in TOGW if the payload is increased. For the payload trade part; the range is taken as a constant (100 km) and the payload is variable (1 kg/1.5 kg/2 kg). At first W_0, the gross weight is estimated as 21.3 kg which is the average of the 6 aircraft chosen. In Table 4, Table 5, and Table 6 the payloads are given as 1, 1.5, and 2 kg respectively.

Table 4. W_0 Calculated with 1 kg Payload.

W_0 (lbs)	W_{crew} (lbs)	$W_{payload}$ (lbs)	W_f (lbs)	W_f/W_0	W_e/W_0	W_0	Difference	W_0 (kg)
9	0	2.205	0	0	0.806	11.339	2.339	4.077
10	0	2.205	0	0	0.801	11.097	1.097	4.53
11	0	2.205	0	0	0.797	10.889	-0.111	4.983
12	0	2.205	0	0	0.794	10.706	-1.294	5.436
13	0	2.205	0	0	0.791	10.543	-2.457	5.889

Table 5. W_0 Calculated with 1.5 kg Payload.

W_0 (lbs)	W_{crew} (lbs)	$W_{payload}$ (lbs)	W_f (lbs)	W_f/W_0	W_e/W_0	W_0	Difference	W_0 (kg)
13	0	3.3075	0	0	0.791	15.815	2.815	5.889
14	0	3.3075	0	0	0.788	15.597	1.597	6.342
15	0	3.3075	0	0	0.785	15.400	0.400	6.795
16	0	3.3075	0	0	0.783	15.221	-0.779	7.248
17	0	3.3075	0	0	0.780	15.056	-1.944	7.701

Table 6. W_0 Calculated with 2 kg Payload.

W_0 (lbs)	W_{crew} (lbs)	$W_{payload}$ (lbs)	W_f (lbs)	W_f/W_0	W_e/W_0	W_0	Difference	W_0 (kg)
16,5	0	4.41	0	0	0.781	20.182	3.682	7.4745
18	0	4.41	0	0	0.778	19.874	1.874	8.154
19,5	0	4.41	0	0	0.775	19.599	0.099	8.8335
21	0	4.41	0	0	0.772	19.353	-1.647	9.513
22,5	0	4.41	0	0	0.769	19.129	-3.371	10.1925

Consequently, the above-given tables and figures determine that as the payload is increased, the total weight of the aircraft increases more than the payload value. This is because as the aircraft is carrying more weight, the aircraft's range will decrease. As a result, so far a mission profile for a UAV is given. The first estimate of the TOGW is calculated based on the mission profile. Payload trade with a constant range is also done to see how the payload is affecting the UAV's total weight. The mission profile is sketched, and tables and figures are plotted.

2.4. Design Lift Coefficient Calculation

Using previous parameters and atmospheric conditions C_L, Reynolds Number and thickness ratio are calculated, then the 4 best airfoils are chosen to satisfy the thickness ratio. These airfoils were compared according to, C_D and C_M values. Maximum speed, stall speed, and best range are evaluated from the results of C_L, C_D, and C_M. The best airfoil is decided by the values that are calculated.

From previous studies, based on the compared UAVs and the aimed mission profile, the Aspect Ratio (AR) was decided to be 15 from the optimized aspect ratio values (17.5, 15, and 12.5) because the Stall Speed (SS) and UAV

Gross Weight at this AR value were achieved at the desired values. Although the UAV Weight decreased at higher Aspect Ratio values (17.5), the Stall Speed increased. On the other hand, although the Stall Speed was lower at lower Aspect Ratio values (12.5), the UAV Weight increased dramatically. Since the determined span value is 3, the Wing Area value was removed from the formula and found to be 0.6 m^2. In this manner, the design lift coefficient is selected for the cruise condition with level flight assumption as given below;

At 3000 feet:

$\rho_\infty = 1.112 \ kg/m^3$

$g = 9.79 \dfrac{m}{s^2}$

$\mu_\infty = 1.758 \times 10^{-5} N.s/m^2$

Where ρ_∞ is Density, g is gravity and μ_∞ is viscosity.

Assumption:

$V_{max} = 33.3 \ m/s = 120 \ km/h$

$W = 8.834 \ kg$

$b = 3 \ m$

Where V_{max} is maximum speed, W is wieght and b is average span

And then Chord Length (c) is calculated as;

$$c = \frac{b}{AR} \tag{2}$$

for   Aspect Ratio (AR) is then

$$AR = \frac{b^2}{S} \qquad (3)$$

Where S is wing area
Consequently;
$S = 0.6\,m^2$ and $c = 0.2\,m$ are found
For Lift Coefficient;

$$C_L = \frac{L}{(\frac{1}{2} \times \rho_\infty \times V_\infty^2 \times S)} \quad for\ L = W \qquad (4)$$

Finally;
$C_L = 0.22$

2.5 Reynolds Number Calculation
For calculating Reynolds Number, stall speed and average chord length are used at standard mean sea level conditions.
At mean sea levell conditions:
$\rho_\infty = 1.225\,kg/m^3$
$\mu_\infty = 1.789 \times 10^{-5}\,N.s/m^2$
Then Re is calculated as;
$$Re = \frac{(\rho_\infty \times V_\infty \times c)}{\mu_\infty} \qquad (5)$$
Where V_∞ is the free flow speed
$Re = 2.36 \times 10^5$
For calculating Reynolds Number at maximum speed and average chord length which is used at 3000 feet conditions:
$Re = 4.21\ x\ 10^5$

2.6. Thickness Ratio Calculation
Calculated Mach number for maximum speed at cruise conditions.
$$M = \frac{V_\infty}{a} \qquad (6)$$

where M is "Mach number" and a is the speed of sound.
$V_{max} = 33.3\,m/s = 120\,km/h$
$a = 336.4\,m/s$ (@3000 feet)
$M = 0.1$

Raymer et al [8] has provided a historical trend line of thickness ratio to design Mach number. By using design Mach number from the mentioned study as 0.1, thickness ratio is found as 0.12 as given below;
$t/c = 0.12$

2.7. Airfoil Selection
According to the thickness ratio previously found, 4 different airfoils to satisfy this value are selected. The selected airfoils are; NACA23012, NACA0012, NACA4412, NACA2412. Airfoils are selected from airfoil tools [10, 11]. As presented in Table 7, Using

maximum speed condition at 3000 feet, Reynolds Number is found as $Re = 4.21\ x\ 10^5$. Parametrically, the Reynolds for each airfoil and AoA, C_D and C_M can be found. For C_D and C_M values, the AoA is taken as 0. For the AoA that yields the maximum C_L is chosen [12, 13].

2.8. Best Range Condition
For a general case:
$$\frac{D}{V} = \frac{(C_D \frac{1}{2}\rho V^2 S)}{V} = 2\rho S V C_D =$$
$$\frac{1}{2}\rho S \sqrt{\frac{W}{\frac{1}{2\rho S}}} \frac{C_D}{C_{L_{max}}^{1/2}} \qquad (7)$$

Where C_D is drag coefficient, D is a drag, $C_{L_{max}}$ is Maximum Lift Coefficient and V is speed. For a given altitude and weight, the range is maximum when $\frac{C_D}{C_{L_{max}}^{1/2}}$ is minimum, hence $\frac{C_{L_{max}}^{1/2}}{C_D}$ maximum. It should be underlined that the NACA4412 has the biggest value from all 3 airfoils four digits.

2.9. Best Stall Speed Condition
The angle of attack (AoA) is decreased, as is the angle between the chord line of the wing and the relative wind, to explain the stall and best stall speed. As all aerodynamic forces are AoA functions, as seen in Figure 2, this is one of the essential parameters of a fixed-wing aircraft.
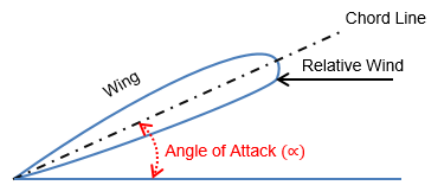
Figure 2. Graphical Description of AoA [14].

The stall can be defined as is an unwanted phenomenon that occurs when the lift is lost and the AoA can be defined as the angle between the oncoming air or relative wind and a reference line on the wing [14].
The biggest C_L value at optimum AOA gives the best stall speed condition. This is simply because the aircraft's velocity will be very low to generate lift so the lift coefficient should be high enough to lift the weight of the aircraft. NACA4412 has the biggest C_L value of all 4

Table 7. Comparison of Selected Airfoils.

	C_{Lmax}	$C_{D,0}$	$C_{M,0}$	$C_L^{1/2}/C_D$	α_{CLmax}
NACA23012	1.0843	0.00587	-0.0067	177.3931	9
NACA0012	0.6195	0.0054	0	145.7562	5
NACA4412	1.2002	0.00678	-0.1032	161.5835	7
NACA2412	0.803	0.00568	-0.0525	157.7646	5

airfoils. In this manner, C_{Lmax} is re-written in the form given in formula (8)

$$C_{L_{max}} = \frac{L}{(\frac{1}{2} \times \rho_\infty \times V_{stall}^2 \times S)} \quad \text{for L = W} \quad (8)$$

Where W is total weight. In this state, V_{stall} is the stall speed.

$C_{L_{max}} = 1.2$ (for NACA4412)

$W = 8.834 \text{ kg}$

$S = 0.6 \text{ m}^2$

And finally, stall speed is found as;

$V_{stall} = 14.71 \text{ m/s} (52.96 \text{ km/h})$

2.10. Maximum Speed Condition

Maximum speed for an aircraft is a requirement for aircraft that can fly at supersonic speeds. It should be declared that all the selected UAVs are not capable of supersonic flights. However maximum airspeed could be obtained during the steady, horizontal flight when the AoA, a=0.

$L = W$

$T = D$

$D/L = C_D/C_L$ (9)

And setting $T = T_{max}$ to obtain maximum speed;

$T_{max} = D$

$T_{max} = (C_D/C_L) W$ (10)

Where T_{max} is Maximum Engine Thrust, C_L is lift coefficient.

Since the weight of the aircraft W is constant, the result is obtained while C_D/C_L is maximum. NACA4412 airfoil could be selected to fit the requirement.

Conclusionally, using variables from previous studies, thickness ratio is found. Using thickness ratio, 4 best airfoils to satisfy this ratio are chosen. , C_D and C_M values were found using

relevant formulas as forementioned. Those coefficient values were needed to find, which airfoil gives the best stall speed and the best range condition. NACA 4412 airfoil is selected as the best airfoil. The selected airfoil has the best range condition and low stall speed condition, compared to the selected airfoils. The characteristics of both wing and fuselage are to be found. Both are compared and the one that benefits more is chosen.

3. EXPERIMENTAL FINDINGS

A parametric approach was introduced in the current study for reaching the optimal airframe body. The aspect ratio of a wing in this manner is the ratio of its span to its mean chord. The square of the wingspan divided by the wing area is equal to that. The aspect ratio was decided to be 15 from the optimized aspect ratio values (17.5, 15, 12.5) because the Stall Speed and UAV Gross Weight at this Aspect Ratio value were achieved at the desired values.

3.1. Aspect Ratio

The aspect ratio of a wing in aeronautics is the ratio of its span to its median (mean) chord. The square of the wingspan divided by the wing area is equal to that. The aspect Ratio was decided to be 15 from the optimized aspect ratio values (17.5, 15, 12.5) because our Stall Speed and UAV Gross Weight at this Aspect Ratio value were achieved at the desired values.

$$AR = \frac{b^2}{S} \quad (11)$$

For the 'Sailplane' and based on the UAVs stall speeds and the mission profiles were compared as given in Table 8. Finally;

$b = 3 \text{ m}$

$S = 0.6 \text{ m}^2$

Table 8. Comparison of Aspect Ratio Values [9].

W_0	C_L	C_D	Aspect Ratio	b (Span) (m)	S (Wing Area) (m^2)	λ (Taper Ratio)	C_{root} (m)	C_{tip} (m)	V (Stall Speed) (m/s)	V (Stall Speed) (km/h)
From Weight to Stall Speed Naca4412 @8 Degree AoA										
8.83	1.2	0.02	17.5	3	0.51	0.45	0.236	0.106	15.89	57.21
From Weight to Stall Speed Naca4412 @7 Degree AoA										
8.83	1.2	0.02	15	3	0.60	0.45	0.276	0.124	14.71	52.96
From Weight to Stall Speed Naca4412 @6 Degree AoA										
8.83	1.12	0.01	12.5	3	0.72	0.45	0.331	0.149	13.93	50.15

3.2. Taper Ratio

In the aspect, ratio-quarter chord sweep degrees graph, the quarter chord sweep degree is obtained as 30 degrees concerning the aspect ratio and in the taper ratio-quarter chord sweep degrees graph, the taper ratio is obtained as proportional to quarter chord sweep degrees 0.15 [15].

The tip chords become shorter and thereby alleviate the undesirable consequences of the rectangular wing of the constant-chord. In fact, for an unswept wing, a taper ratio of 0.45 almost virtually eliminates these results, producing a distribution of lifts somewhat close to the perfect elliptical.

For $\lambda = 0.45$
Root chord $= 0.276$ m
Tip chord $= 0.124$ m

It is therefore considered that 25 percent of the mean aerodynamic chord (MAC) from the leading edge is the wing aerodynamic center and that 40 percent of the mean aerodynamic chord is the wing center of gravity, as seen in Figure 3.
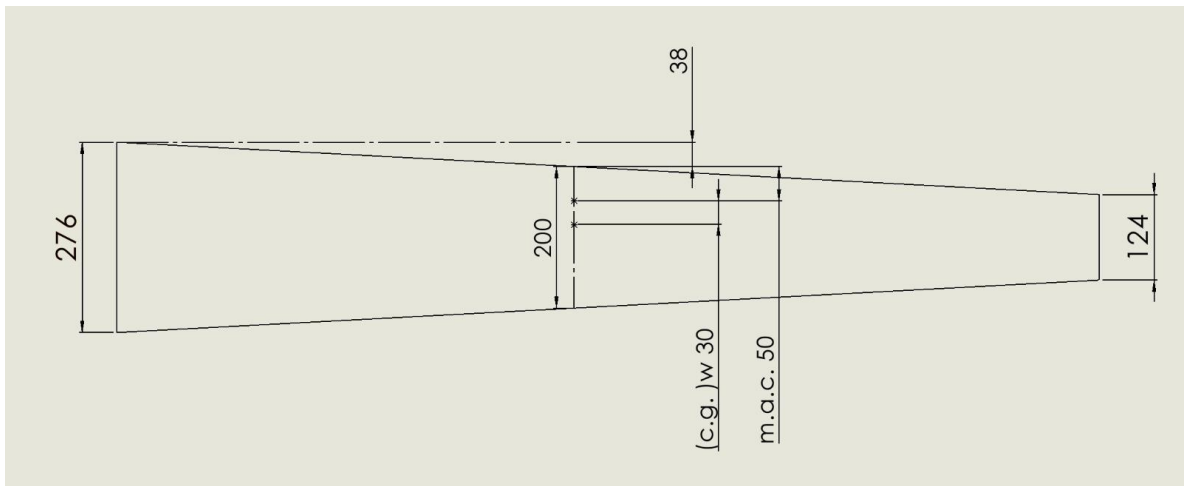
Figure 3. The geometry of the wing, indicating the mean aerodynamic center and wing gravity center positions.

3.3. Wing Twist

The wing twist is basically used for eliminating tip-stall and adjusting the lift distribution to simulate an ellipse.

In order to avoid tip stall and to revise the lift, a wing twist is used. Wings are usually bent between zero and five degrees. The more twist required at the outline lift coefficient to produce an acceptable lift circulation, the more unusable wing can perform at other lift coefficients. For this purpose, it is important to prevent significant volumes of twist (much more than 5 deg.) [16]. The wing strategy is vital, especially for roll and bank angle maneuvers as per Concilio et al [17] in terms of the effectiveness of wing twist morphing as a roll control strategy. Albeit, for initial design purposes, twist optimization for an arbitrary wing platform is very difficult. Historical data calculations are used and the twist angles are compared and the best fitting degree is chosen as 3.

3.4. Dihedral

With reference to the horizontal view from the front, the wing dihedral is the angle of the wing. As the aircraft banks to the left or right, it adds lateral stability. From historical records, the dihedral angle should be calculated, then updated after the design plan review. From dihedral historical data [9] 2 to 4 degrees are given for unswept mid-wing aircraft. Based on the meticulous calculations, it's decided to "0" degrees for dihedral.

3.5. Wing Incidence Angle

The wing incidence angle of the wing is the pitch angle of the wing relative to the fuselage. If the wing is not inverted, the incidence is essentially the angle of the wing's airfoil between the fuselage centerline and the chord lines.

Mainly cruise flight conditions, but also for some other flight stages the wing incidence angle is designated to minimize the drag. The incidence angle is selected for the conditions such that the wing is in the correct position of AoA of the designed condition where the fuselage is at the AoA for minimum drag. It is worth noting that, "0" degrees with the lowest value of drag was chosen for the incidence angle in this study.

3.6. Wing Vertical Location

The mid-wing arrangement provides the least resistance, as the fuselage is designed as roughly circular and hatches are not used [18]. To attain reasonable interference friction with a circular body design, the high and low wing layouts must use cowls or fairings.

It is noteworthy that some of the ground clearance benefits are provided by the mid-wing configuration rather than those of the high-wing. To allow the carrying of rockets, missiles, and usually fuel tanks under the wing, many fighter aircraft are mid-winged. Besides, from a maneuverability perspective, the mid-wing layout may be accepted as a superior configuration for aerobatic maneuverability based on observations that a mid-wing arrangement is widely preferred during normal flight, the dihedral normally needed for acceptable handling characteristics in a low-wing configuration would behave in the wrong direction during inverted flight, making it impossible for smooth aerobatic maneuvers. In addition, the high or low wings' effective-dihedral contribution makes it impossible to execute high-sideslip maneuvers, such as the knife-edge pass.

3.7. Wing Tips

Two influences on subsonic aerodynamic performance are the shape of the wing-tip. The shape of the tip affects, but only to a small degree, the wet region of the aircraft. The influence of the shape of the tip on the lateral differentiation of the tip vortices is a much more important consequence. This is essentially decided by the ease with which the high-pressure air will "escape" along the wing's upward tip on the bottom of the wing.

A slightly-rounded tip, as seen in Figure 4,, allows air to flow around the tip easily. It is rendered more difficult by a tip with a sharp point, thereby reducing the drag caused. Any type of sharp edge is used for most of the new low-drag wing-tips. In fact, because of the sharp edges where the upper and lower surfaces finish, even a plain cut-off tip offers less drag than a rounded-off tip.

Except that the top is curved up or down to maximize effective span without increasing the real wingspan, the "dropped" and "upswept" wing-tips are close to the Hoerner wingtip. The impact described is identical to that used by

endplates, as discussed below. The drag is just as impacted by the wing's sweep.

The tip vortex appears to be centered roughly at the wing-trailing tip's edge, so a back-swept aft-swept wing-tip tends to have weaker drag, with a greater wingspan from the trailing edge. The back-swept wing-tip, however, continues to raise the load of the wing torsion.
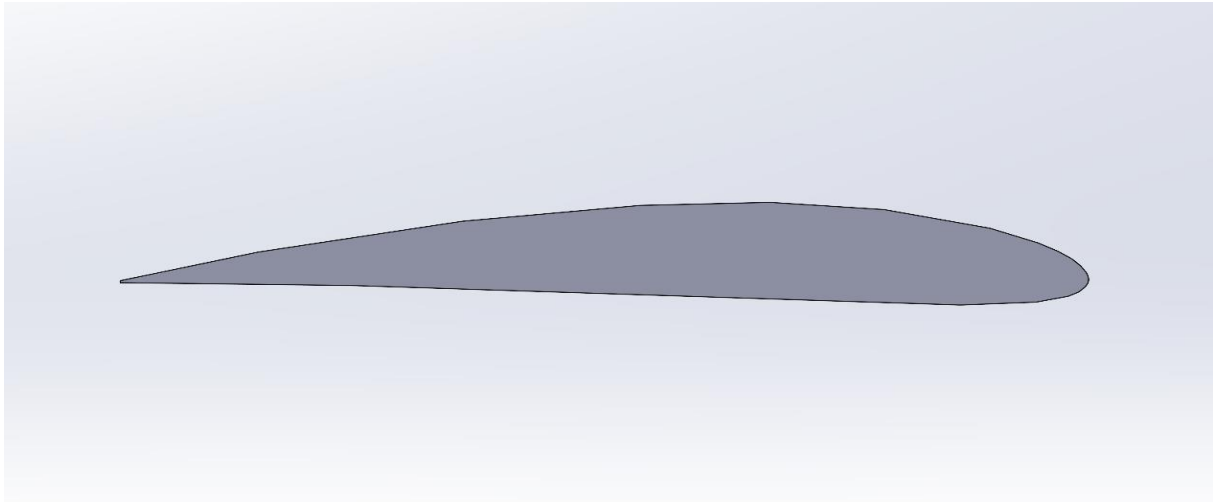
Figure 4. Wing Side View.

In Figure 5 and Figure 6 the designed wing is seen from different angles respectively.
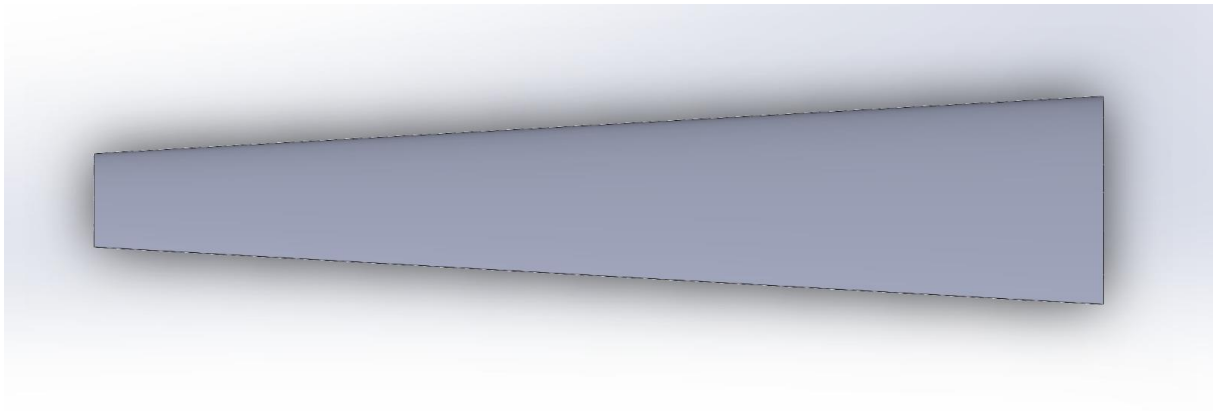
Figure 5. Wing Top View.
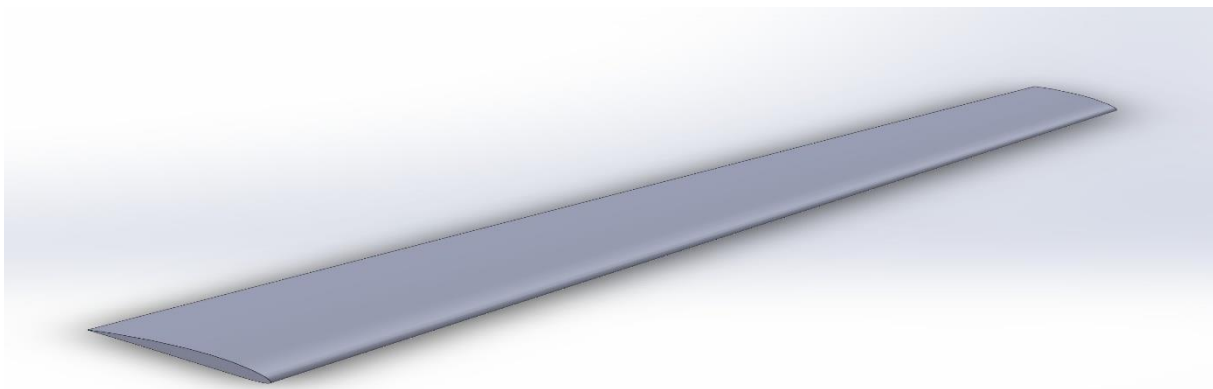
Figure 6. Wing Plan View.

3.8. Fuselage

The designed fuselage has a max outer diameter of 150 mm, a max inner diameter of 130 mm, and a max length of 900 mm. As an innovative approach, the pressurized air will be used as propelling system. Pressurized air will be used for UAV movements of 3 axes (pitch, yaw, and roll) included in the payload. At 30 bar air has a density of 38.65 kg/m^3. 5 liters of air is enough for the mission and it weighs 0.193 kg. For payload whose density has 1750 kg/m^3 and 2 kg will cover 1.142.857 mm^3 of volume. The body is designed as a pressurized tank as shown in Figure 7, Figure 8, and Figure 9 respectively.
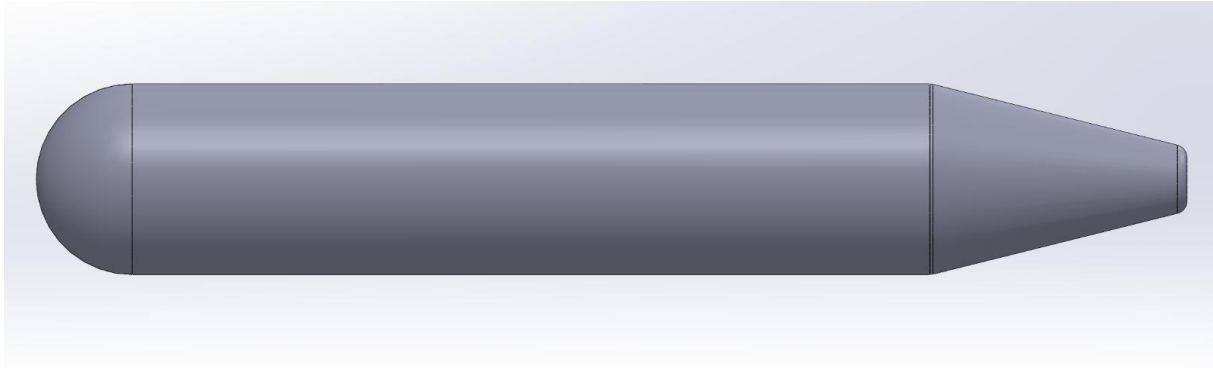
Figure 7. Fuselage Right View.
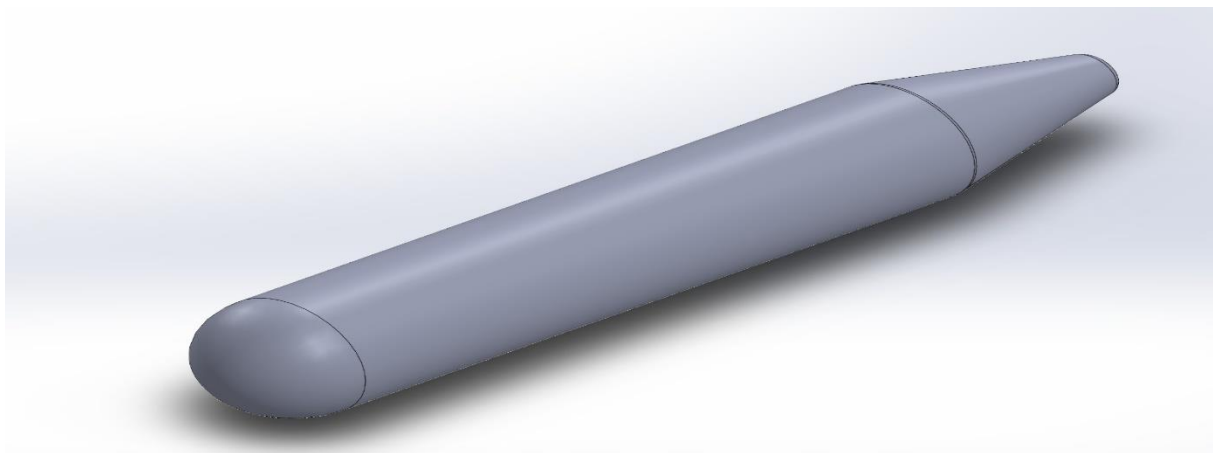
Figure 8. Fuselage Isometric View.

Figure 9. The Location of Payload and Pressurized Air Tank.

93

3.9. Center of Gravity

The center of gravity (cg) has crucial importance for the three-axis movement of the air vehicles. Many accidents were due to uncontrolled cg [20].

$$\tilde{x} = \frac{x_{fuselage} \cdot W_{fuselage} + x_{payload} \cdot W_{payload} + x_{pressurized\ air\ tank} \cdot W_{pressurized\ air\ tank}}{W_{fuselage} + W_{payload} + W_{pressurized\ air\ tank}} \quad [21] \qquad (12)$$

Where $\tilde{x}$ is the center of mass, $x_{fuselage}$ is the distance from the nose, $W_{fuselage}$ is the weight of the fuselage, $x_{payload}$ is payloads distance from the nose, $W_{payload}$ is the weight of the payload, $x_{pressurized\ air\ tank}$ is the distance of the pressurized tank from the nose, and $W_{pressurized\ air\ tank}$ is the weight of the pressurized tank.
$\tilde{x} = 333$ mm (without wing)
According to these determined locations (fuselage, payload, and pressurized air tank) the center of mass of these important weight values [21] was found to be 333 mm. To this center of mass; The assembly was made to coincide with the aerodynamic center of the wing (333 mm from the nose).

$m.\,a.\,c._{wing} = 333$ mm

By adding the weight of the assembled wings, the new center of gravity has been found so that the new center of mass is 348 mm from the nose of the aircraft. These data will be taken into account in the next stage, the tail design.
$\tilde{x} = C.\,G._{Wing+Fuselage} = 348$ mm as it is shown in Figure 10
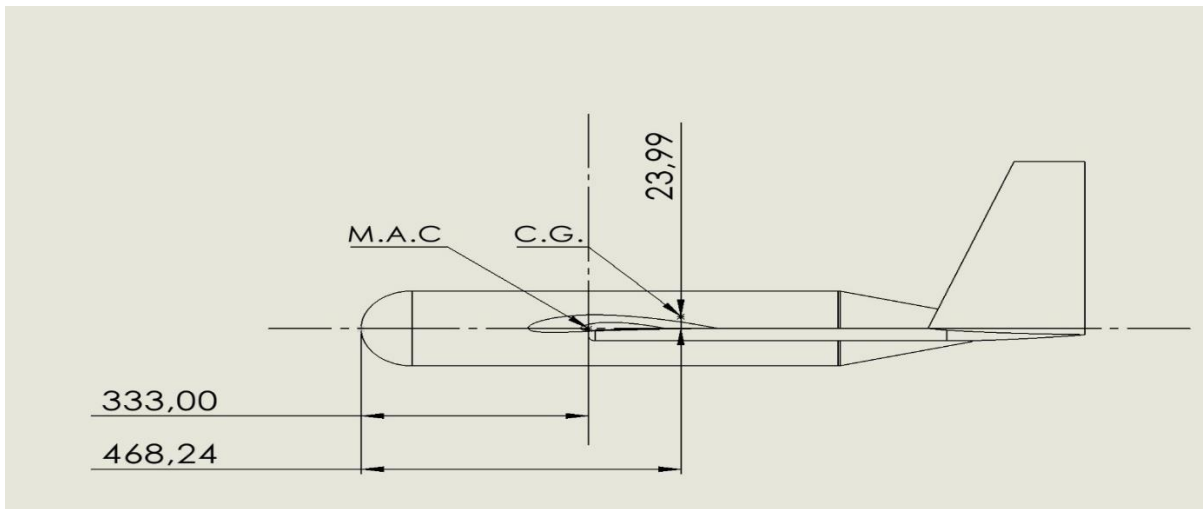
Figure 10. Points of the Mean Aerodynamic Center (MAC) and cg.

3.10. Horizontal and Vertical Tail Size

High boom tail aircraft is characterized by two longitudinal booms (elongated engine compartment-like fuselages). In accordance with Sadraey et al [19], it may include auxiliary components such as fuel tanks, booms other components for supporting the structure.
Ina pusher configuration propeller system, even if it is a piston engine, jet engine, single-engine or twin-engine, a conventional drive requires the propeller or exhaust to be moved too far, which requires a very long driveshaft or jet tube, hence reducing propulsion efficiency. On the contrary, the high boom tail configuration provides a much shorter and more efficient setup.
Tip results in the tailplane, on the other hand, being avoided and supported at both sides, so it becomes smaller and lighter. Furthermore, span-loading across the wing will significantly decrease structural forces between the booms and total weight.

The scale of the tail is one of the most empirical and least accurate elements of the method of airplane construction. Providing longitudinal stabilization is the primary function of the horizontal tail. The equations are described by tail volume ratios as follows: [21]:

For horizontal tail:
$$V_{HT} = \frac{l_{HT}S_{HT}}{cS} \qquad (13)$$

For vertical tail:
$$V_{VT} = \frac{l_{VT}S_{VT}}{bS} \qquad (14)$$

where the horizontal and vertical tail volume measurements, respectively, are V_{HT} and V_{VT}. The horizontal gaps between the aircraft's center of gravity and the aerodynamic center of the horizontal and vertical tail are l_{HT} and l_{VT}. S_{HT} is the horizontal tail's planform area, S_{VT} is the vertical tail's side view area, c is the wing's mean aerodynamic chord, b is the wingspan, and S is the area of the wing planform.

The proposed values of these volume ratios, based on historical single-engine general aviation aircraft, are:
$$V_{HT} = 0.5, V_{VT} = 0.02$$

Since the horizontal distance between the center of gravity of the airplane and the aerodynamic entry of the horizontal tail is approximately %60 of the fuselage length for the vertical tail because minor distances are neglected therefore both are assumed equal.
$$l_{HT} = l_{VT} = 0,646 \qquad (15)$$
From Volume Ratio Equations:
$$S_{HT} = 0.092 \text{ m}^2$$
$$S_{VT} = 0.056 \text{ m}^2$$

Thus, if the horizontal tail has a lower aspect ratio than the wing, when the wing stalls, the tail still has some control authority [22]. To achieve this gain, an aspect ratio less than the wing for the horizontal tail is picked, so AR= 8 and λ= 1 for the taper ratio.
Therefore, the span of the horizontal tail b_t is:

$$b_t = \sqrt{S_{HT}AR_{HT}} = 0.86 \text{ m} \qquad (16)$$

The tail root chord crt and the tail tip chord are obtained from the ratio that is given below;

$$c_{rht} = c_{tht} = c = 0.11 \text{ m} \, [21] \qquad (17)$$

The spanwise location of the mean aerodynamic chord for the horizontal tail is:

$$y_{HT} = \frac{b_t}{6}\frac{1+2\lambda}{1+\lambda} = 0.22 \text{ m} \qquad (18)$$

and the mean aerodynamic chord for the horizontal tail is:

$$c_{HT} = \frac{2}{3}c_{rt}\frac{1+\lambda+\lambda^2}{1+\lambda} = 0.10 \text{ m} \qquad (19)$$

For vertical tail AR= 2. is chosen. Therefore:

$$h_{VT} = \sqrt{S_{VT}AR_{VT}} = 0.33 \text{ m} \qquad (20)$$

The root chord and the tip chord of the vertical tail are obtained from the ratio given below;

$$C_{rvt} = 0.23 \text{ m}$$
$$C_{tvt} = 0.10 \text{ m}$$

Referred to the root chord, the vertical position of the mean aerodynamic chord of the vertical tail is :

$$z_{HT} = \frac{2h_{VT}}{6}\frac{1+2\lambda}{1+\lambda} = 0.15 \text{ m} \qquad (21)$$

The mean aerodynamic chord for the vertical tail is:

$$c_{VT} = \frac{2}{3}c_{rvt}\frac{1+\lambda+\lambda^2}{1+\lambda} = 0.17 \text{ m} \qquad (22)$$

In Figure 11 and Figure 12, the obtained values are illustrated on the body.
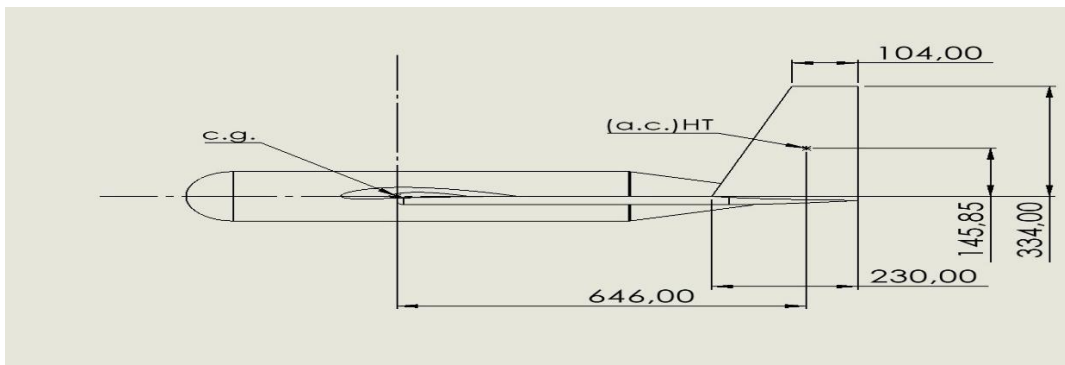
Figure 11. Side View – Fuselage and Horizontal Tail.
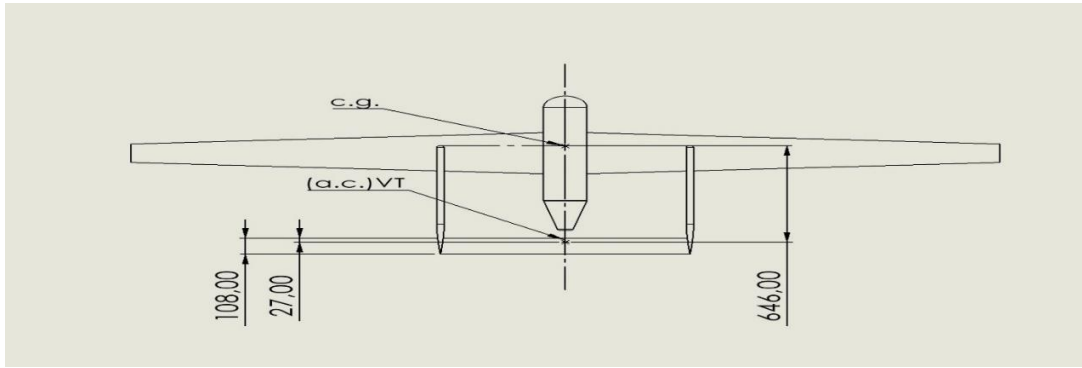
Figure 12. Plan View – Fuselage and Horizontal Tail.

It should not be underestimated that the horizontal and vertical tail calculations as empennage depends on Tail Volume Coefficients [23].

It can be seen that the selection was performed for symmetric airfoil as the horizontal and vertical tail should behave similarly when at a positive or negative AoA [13] as provided in Table 9.

Table 9. Tail Airfoil Comparison.

	Cl_{max}	$Cd_{\alpha=0}$	$(Cl/Cd)_{max}$	α_{stall}
NACA0006	0,77	0,004	78,726	7
NACA0009	1,284	0,005	99,625	12
NACA0012	1,562	0,005	107,754	16
NACA0015	1,653	0,006	107,769	18
NACA0018	1,64	0,006	108,472	18
NACA0021	1,589	0,007	103,992	19
NACA0024	1,526	0,007	95,12	19

In Figure 13 and Figure 14 the airfoil analysis results are shown. The calculation-based study was performed using XFLR5 wing profile analysis software.
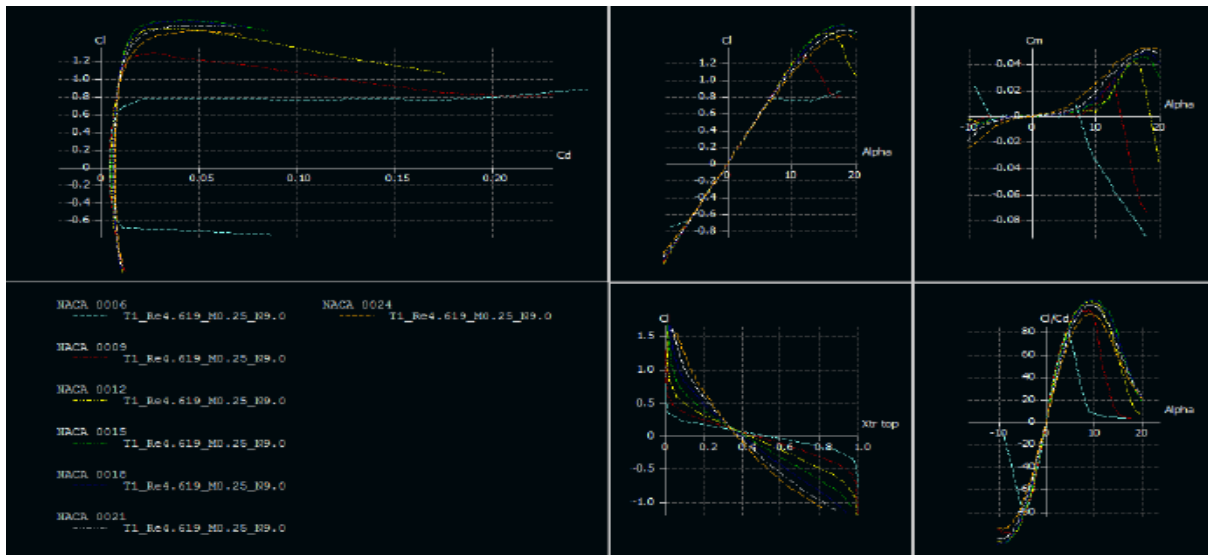
Figure 13. Airfoil Analysis Results with XFLR5.
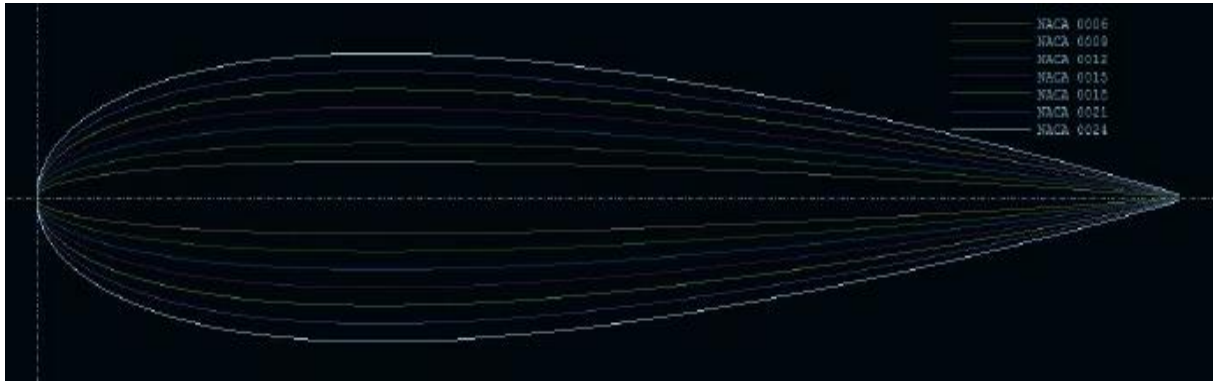
Figure 14. Airfoil Shape Comprised.

The justifications for both Horizontal tail and vertical tail are given as follows;
Horizontal Tail Justifications:
• Horizontal tail should never stall, at least stall later than the wing
• Maximize CLmax
• Maximize stall angle
• Minimize drag
• Minimize size

It is decided NACA0009 according to these and the table because of tail size.
Vertical Tail Justifications:
• Minimize structure and weight
• Minimize size-thickness
It is decided NACA0006 according to these and the table. However, the AoA data is getting irregular. Thus, Naca0009 values are more suitable. As a result, the high boom tail which is shown in Figure 15 was designed.
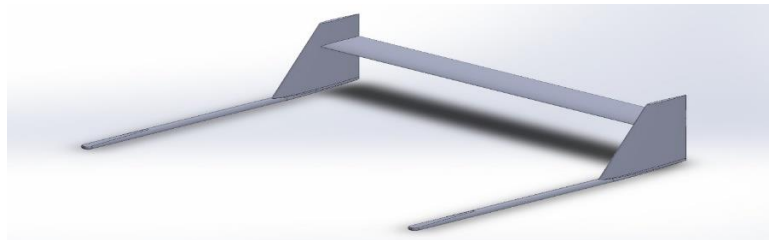
Figure 15. High Boom Tail.

3.11. Better Weight Estimation
According to all calculations, the UAV exterior design was drawn using Solidworks The appropriate material density and properties were entered, and the locations of the details (Payload, Air Pressure Tank) that would affect the weight were determined. The weights and centers of gravity of the details that will affect our entire balance were taken from Solidworks. Data has been entered parametrically and the better weight estimation of our entire shape has been renewed once again. At the same time, the new center of gravity location was found as provided in Table 10.

Table 10. Weight, Longitudinal, and Vertical C.G. Location of Each Component.

Component	Weight (gr)	C.G. Horizantol Location (mm)	C.G. Vertical Location (mm)
Fuselage	2313	428.33	0
Wing	2375	364.7	6.8
Tail Section (H.T. And V.T. have been designed as one component	1429	886,03	113.17
Pressurized Air	200	450	0
Payload	2000	210	0
Average	8317	467.812	23.994

According to the data in Table 10
Better Estimated Weight:
$W_0 = 8317$ kg
Estimated Center of Gravity (C.G.) Coordinate
is found as;

$$[\tilde{x}, \tilde{y}] = [(467.8), (23.99)] \text{ mm} \qquad (23)$$

Previously, the Mean Aerodynamic Center (MAC) Point was calculated as 333 mm from the nose. After better weight estimation studies the new Horizontal Center of Gravity point is calculated as 468 mm from the nose.

The rigid "longitudinal stability" criteria require that behind the "center of gravity" or "aircraft neutral point" the "aircraft aerodynamic center" is never permitted to be. In terms of the non-dimensional derivative, for an aircraft to be statically longitudinally stable, the rate of change of the pitching moment concerning the AoA must be negative [24]. The horizontal

center of gravity (x_{cg}) is found 468 mm and the aerodynamic center of the aircraft (x_{ac}) is found 333 mm in previous studies. The aircraft satisfies these requirements hence the aircraft is stable so relocating or resizing certain components to meet the stability criteria is not needed.

$$C_{M_{a_w}} = C_{L_{a_w}}\left(\frac{x_{cg}}{x} - \frac{x_{ac}}{x}\right) \qquad (24)$$

Notably, the CG is significantly ahead of the lift center for fixed-wing aircraft. The lift still turns the aircraft nose-down due to this structural positioning, so nose-up aerodynamic force whose downward direction must be generated on the horizontal tail surfaces in order to stabilize the aircraft [25].
The finalized aerodynamic shape of the UAV is provided in Figure 16, Figure 17, and Figure 18 from different angles.
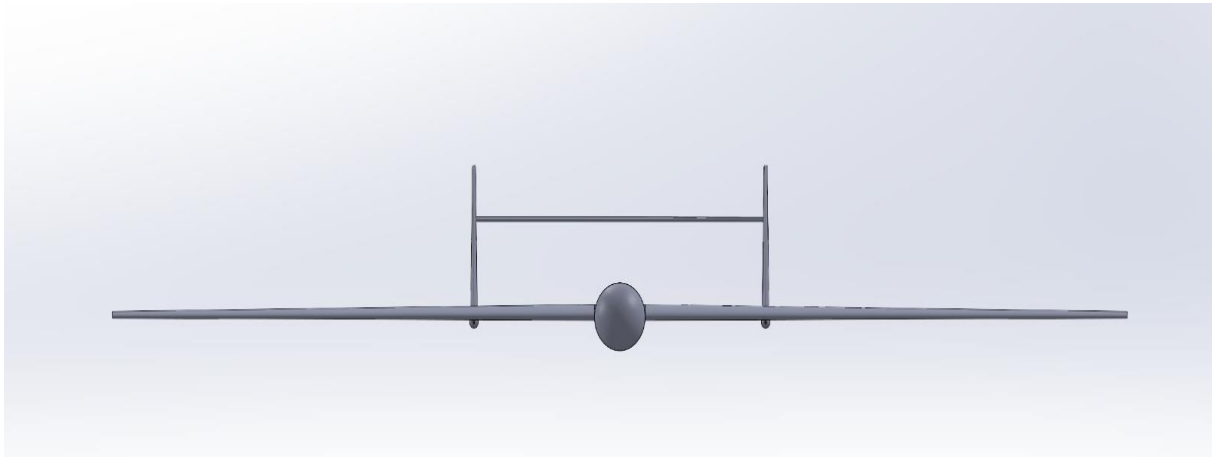
Figure 16. Front View of the UAV.
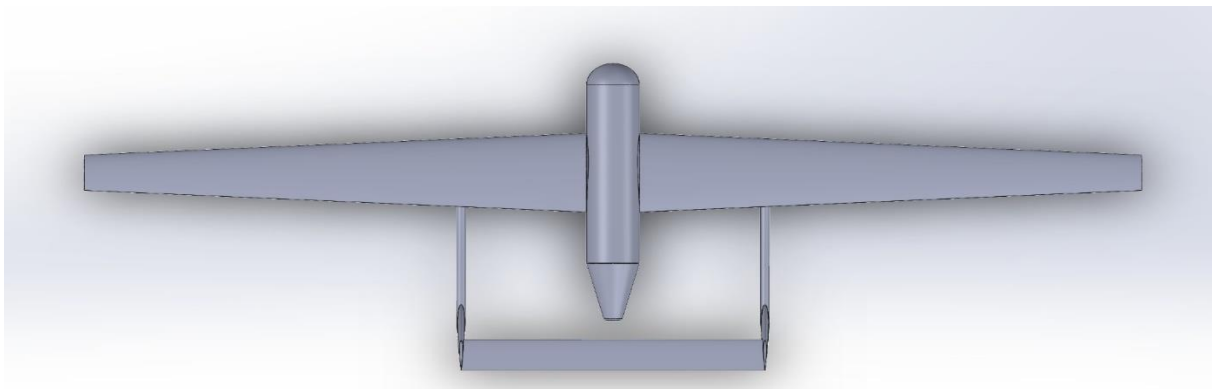
Figure 17. Top View of the UAV.
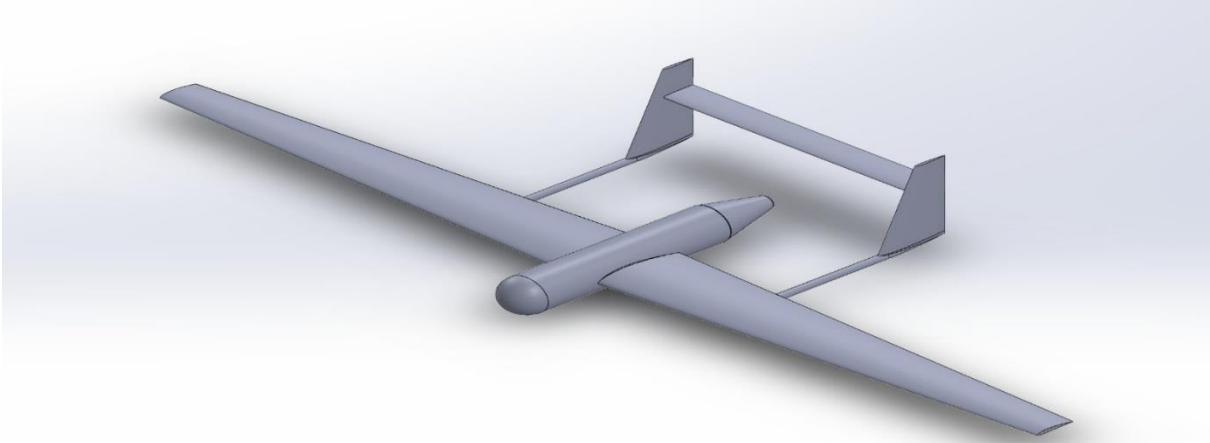
Figure 18. Isometric View of the UAV.

It is noteworthy that, the qualification of the UAV will be performed by the relevant Country Airworthiness Authority (CAA) [26, 27].

3.12. The Operational Environment of UAVs and the Potential Adverse Impacts of Implementation of the Novel Technologies
The UAV which is subject to this study is designed for severe environmental conditions that require detailly planned and realized specifications [28] for meeting the airworthiness regulations. For example, icing is an important issue that needs to be diminished for flight safety. There are some theoretical and practical studies for diminishing the hazard of icing risk [29]. It needs to be underlined that, UAVs are utilized for very significant and important tasks, and their efficiency and long-term viability are critical to their missions [30]. They are preferred due to the convenience they provide, especially in dangerous and risky applications and locations where human use is inefficient and takes a long time [31]. Moreover, the rising cost of petroleum fuels, as well as growing environmental concerns about fossil fuel pollution, have prompted the aviation sector, particularly propulsion manufacturers, to pursue research on reducing fuel consumption and emissions, as well as improving engine efficiency [32]. The CAAs are top-level coordination centers that regulate the operations of the UAVs under the country's laws and aviation rules [33]. Any violence or misbehavior is subjected to relevant airworthiness authorities' law enforcement.

The competition in the aviation industry is fierce. Naturally, this competition forces aircraft manufacturers, maintenance organizations, and airliners to implement the newest technologies into their businesses. The compressed air used as thrust is a novel technology that might be used instead of fossil fuel or batteries. On the other hand, The International Civil Aviation Organization (ICAO) warns in its "Global Aviation Safety Plan 2020-2022" that new technology and concepts may have a negative influence on flight safety unless they are well-developed [34]. The Aviation industry has witnessed two significant accidents originated of implementation the Maneuvering Characteristics Augmentation System (MCAS) in Boeing-737 Max aircraft [35]. Despite the fact that the subject of this study is a UAV, which is smaller than commercial passenger aircraft, it should be noted that every novel technology implementation requires meticulously organized and executed validation tests governed by national/international airworthiness organizations.

4. RESULTS
In the present study, a calculational determination was performed in terms of designing a UAV. Some concluding remarks obtained from the results and discussion of the present study may be provided as follows;

• The wing, fuselage, and tail parts of the UAV were designed in the most appropriate way to the mission profile. Stability was selected as the main concern naturally and the design was shaped with this necessity.

• The better size estimation changed the geometry of the UAV and a final decision was made.

- Mid-wing, twin-tail, and comparatively light body of the UAV will have 3 axis stability and provide many advantages, especially in terms of operational cost.
- During manufacturing, the surface roughness of the aerodynamic surfaces will be optimized per the parameters of the machine.

As a concluding remark, it is noteworthy that the designed UAV is subjected to manufacturing with additive manufacturing technologies which provides opportunities for one-stop-machining and building of complex geometries.

The information regarding the weight estimation, the wing selection, and surrounding geometry of UAVs have significant impacts on the operation cost, range, and mission time. In this manner, the findings in this study can be used for an adequate estimated calculation of an additively manufactured loiter munition UAV.

CONFLICT OF INTEREST
The authors declare no conflict of interest.

REFERENCES
1. Kasapoğlu, C., Kırdemir, B., "The Rising Drone Power: Turkey On The Eve Of Its Military Breakthrough", Centre for Economics and Foreign Policy Studies, Pages 3-32, New-York, 2018.

2. Slijper, F., "Where to draw the line. Increasing Autonomy in Weapon Systems–Technology and Trends", Page 1-24, PAX Publications, Utrecht, 2017.

3. Slijper, F., Beck, A., and Kayser, D., "State of AI.Artificial intelligence, the military and increasingly autonomous weapons", PAX Publications, Utrecht, 2019.

4. Sathyamoorthy, D., "A Review of Security Threats of Unmanned Aerial Vehicles and Mitigation Steps", The Journal of Defence and Security. Vol. 6, Issue 1, Pages 81-97, 2015.

5. Zwijnenburg, W., Postma, F., "Unmanned Ambitions. Security implications of growing proliferation in emerging military drone markets", PAX Publications, Utrecht, 2018.

6. Internet: Gettinger, D., Michel, A. H., Loitering Munitions. https://dronecenter.bard.edu/files/2017/02/CSD-Loitering-Munitions.pdf, March, 2022.

7. Chamola, V., Kotesh, P., Agarwal, A., Naren, Gupta, N., & Guizani, M., "A Comprehensive Review of Unmanned Aerial Vehicle Attacks and Neutralization Techniques", Ad Hoc Networks. Vol. 111, Issue 102324, Pages 1-20, 2020.

8. Gudmunsson, S., "General Aviation Aircraft Design: Applied Methods and Procedures", Page 21, Elsevier, Oxford, 2014.

9. Raymer, D. P., "Aircraft Design: A Conceptual Approach", American Institute of Aeronautics and Astronautics, Pages 17-21, AIAA, Washington, D.C., 1992.

10. Shams, T.A., Shah S.I.A., Javed, A., Hamdani, S.H.R., "Airfoil Selection Procedure, Wind Tunnel Experimentation and Implementation of 6DOF Modeling on a Flying Wing Micro Aerial Vehicle", Micromachines, Vol. 11. Issue 553, Pages 1-31, 2020.

11. Arra, A., Anekar, N., Nimbalkar, S., "Aerodynamic effects of leading edge (LE) slats and slotted trailing edge (TE) flaps on NACA-2412 airfoil in prospect of optimization", Materials Today: Proceedings, Vol. 44, Pages 587-595, 2020.

12. Eppler, R. "Airfoil Design and Data", Pages 1-568, Springer, Heidelberg, 1990.

13. Internet: Airfoil Tools, http://airfoiltools.com, March, 2022.

14. Saraçyakupoğlu, T. "The Organizational Accidents in Aviation: An Investigation of B-737 Max Aircraft Accidents from the Engineering Perspective", Mühendis ve Makina, Vol. 61, Issue 701, Pages 241-261, 2020.

15. Filippone, A., "Data and performances of selected aircraft and rotorcraft", Progress in Aerospace Sciences, Vol. 36, Issue 8, Pages 629–654, 2000.

16. Wu, D., Yeo, K. S., & Lim, T. T., "A numerical study on the free hovering flight of a model insect at low Reynolds number", Computers & Fluids, Vol. 103, Issue 1, Pages 234–261, 2014.

17. Concilio, A., Dimino, I., Lecce, L., Pecora, R., "Morphing Wing Technologies Large Commercial

Aircraft and Civil Helicopters", Pages 1-970, Elsevier, Oxford, 2018.

18. Blair, M., Robinson, J., McClelland, W.A., & Bowman, J.C., "A Joined-Wing Flight Experiment" Air Force Research Laboratory, Pages 1-213, Ohio, 2008.

19. Sadraey, M.H., "Aircraft Design: A System Engineering Approach", Pages 1-570, Wiley, Sussex, 2013.

20. Boyd, D. D., "General aviation accidents related to exceedance of airplane weight/center of gravity limits", Accident Analysis & Prevention, Vol. 91, Pages 19–23, 2016.

21. Anderson, J. D., "Aircraft Performance and Design", Pages 1-596, McGraw-Hill, Boston, 1999.

22. Etkin, B., Reid, L. D., "Dynamics of Flight: Stability and Control", Pages 1-395, Wiley, New-York, 1996.

23. Kundu, A.K., "Aircraft Design", Pages 1-650, Cambridge University Press., New-York, 2010.

24. Nelson, R. C., "Flight Stability and Automatic Control", Pages 1-150, McGraw-Hill, New-York, 1989.

25. Liu, Y.,Yang, Z., Deng, J., Zhu, J., "Investigation of fuel savings for an aircraft due to optimization of the center of gravity", Materials Science and Engineering, Vol. 322, Issue 7, Pages 1-5, 2018.

26. Saraçyakupoğlu, T., "Uçuşa Elverişlilik Kural ve Düzenlemelerine Göre, Havacılık Endüstrisinde 3 Boyutlu Üretim Uygulamaları", International Journal of 3D Printing Technologies and Digital Industry, Vol. 4, Issue 1, Pages 53-65, 2020.

27. Saracyakupoglu, T., "The Qualification Of The Additively Manufactured Parts in The Aviation Industry", American Journal of Aerospace Engineering, Vol. 6, Issue 1, Pages 1-10, 2019.

28. Balli, O., "Turbine wheel fracture analysis of Jet Fuel Starter (JFS) engine used on F16 military aircraft", Engineering Failure Analysis, Vol. 128, Pages 1-13, 2021.

29. Ateş, F., Şenol, R., "Hava Araçlarında Buzlanma Risk Derecesinin Yapay Zekâ İle Tahmin Edilmesi", International Journal of 3D Printing Technologies and Digital Industry, Vol. 5 Issue 3, Pages 457-468, 2021

30. Balli, O., Caliskan, H., "On-design and off-design operation performance assessmentsof an aero turboprop engine used on unmanned aerial vehicles (UAVs) in terms of aviation, thermodynamic, environmental and sustainability perspectives", Energy Conversion and Management, Vol. 243, Issue 1, 2021.

31. Akdeniz, H. Y., "A Study on Aerodynamic Behavior of Subsonic UAVs' Wing Sections with Flaps", International Journal of Aviation Science and Technology, Vol. 2, Issue 1, Pages 22-27, 2021.

32. Balli, O., "General aviation and thermodynamic performance analyses of micro turbojet engine used on drones and unmanned aerial vehicles (UAV)", Journal of Aviation Research, Vol. 2, Issue 2, Pages 115-141, 2020.

33. Saraçyakupoğlu, T. "Emniyet İrtifasından Bilgiler: Genel Havacılık, Üretim ve Bakım Süreçleri". ISBN: 978-625-402-030-8, Nobel Akademic Publishing, Ankara, 2020.

34. Saraçyakupoğlu, T., "The adverse effects of implementation of the novel systems in the aviation industry in pursuit of maneuvering characteristics augmentation system (MCAS)", Journal Of Critical Reviews, Vol. 7 Issue 11, Pages 2530-2538, 2020.

35. Saraçyakupoğlu, T., "Havacılıkta Organizasyonel Kazalar: B-737 Max Uçak Kazalarının Mühendislik Perspektifinden İncelenmesi". Mühendis ve Makina, Vol. 61, Issue 701, Pages 241-261, 2020